

Development of a system for testing full-size CMS LGAD sensors

Kyungmin Lee ^a, Hoyong Jeong ^a, Junho Kim ^b, Seokhyeon Lee ^b, Jaebak Kim* ^a,
Jae Hyeok Yoo* ^a

^a*Department of Physics, Korea University, Seoul, 02841, Korea*

^b*Department of Physics, Kyungpook National University, Daegu, 41566, Korea*

E-mail: railroad@korea.ac.kr, jaebak@korea.ac.kr, jaehyeokyoo@korea.ac.kr

ABSTRACT: Low-Gain Avalanche Diode (LGAD) sensors, offering timing resolutions of the order of tens of picoseconds, are being widely adopted in particle physics experiments and related applications. As these applications scale to large numbers of sensors with varying pixel geometries, conventional manual characterization techniques become inadequate for large-scale quality control. We present a modular probe card system for automated electrical characterization of pixelated LGAD sensors, consisting of a probe card, a switching board, precision measurement instruments, and control software. The system supports flexible pixel selection and measurement. Its performance is demonstrated through current-voltage (I-V) and capacitance-voltage (C-V) measurements of a 16×16 LGAD array. A rapid row-wise I-V scan of the full array is completed in approximately 20 minutes, while a pixel-by-pixel I-V scan from 0 to 300 V with a 1 V step requires about 340 minutes. The switching matrix introduces less than 1 nA of leakage current even in a conservative worst-case configuration, remaining small compared with the leakage current of a normal LGAD pixel. The modular architecture and automation capability make the system a practical and scalable solution for large-scale LGAD sensor quality control and distributed testing environments.

KEYWORDS: Timing detectors; Solid state detectors; Performance of High Energy Physics Detectors; Data acquisition circuits

Contents

1	Introduction	1
2	System design for LGAD sensor evaluation	2
3	Probe card	4
4	Mechanics and alignment	5
5	Switching board	8
6	Software Design	10
7	Performance	12
8	Conclusions	15

1 Introduction

The Low-Gain Avalanche Diode (LGAD) is a silicon detector capable of providing precise timing resolution and resistance to high radiation fluence [1]. LGADs have been developed to meet the stringent timing requirements of high-luminosity collider environments. In these settings, extreme pileup conditions make spatial tracking alone insufficient for accurate track–vertex association. By integrating high-precision temporal information with spatial coordinates—a technique known as four-dimensional (4D) tracking—LGADs substantially improve pattern recognition and provide powerful capabilities for pileup mitigation.

The combination of moderate internal gain and inherent radiation hardness makes LGADs the preferred sensor technology for precision timing applications in current and future particle physics experiments. They have been used in the CMS-TOTEM Precision Proton Spectrometer since 2017, with sensors of 50 μm thickness and pixel sizes of $0.5 \times 6 \text{ mm}^2$ and $1 \times 3 \text{ mm}^2$, achieving a timing resolution of 35 ps [2–4]. LGADs are planned for deployment in the High-Luminosity Large Hadron Collider era at the ATLAS and CMS experiments, where the sensors have a thickness of 50 μm with $1.3 \times 1.3 \text{ mm}^2$ pixels and approximately 50 ps timing resolution [5–7]. They are being investigated for use in the HADES fixed-target experiment [8], where a 50 μm thick strip sensor with a timing resolution of 47 ps was studied. There are also variants of LGADs under development, such as the AC-LGAD [9], which enables finer segmentation or a larger fill factor. LGADs have also been selected for the time-of-flight system of the ePIC experiment, featuring sensors with thicknesses below 30 μm , pixel sizes of $1.6 \times 1.6 \text{ mm}^2$, and an approximate timing resolution of 20 ps [10]. Applications of LGADs in space experiments and medical fields are also being investigated, leveraging their high timing precision [11, 12].

For LGAD sensors to be deployed in experiments and applications, their performance must be carefully characterized, and each device must undergo strict quality control (QC) procedures. This is particularly critical for next-generation experiments that will rely on thousands of LGAD sensors, such as those planned for the ATLAS and CMS experiments. Conventional characterization techniques are often time-consuming and resource-intensive, making them insufficient for these next-generation experiments.

Previous studies have reported QC of LGAD sensors using probe cards and switching boards developed for the ATLAS experiment [13, 14]. These systems enable automated current–voltage (I–V) and capacitance–voltage (C–V) measurements of 5×5 and 15×15 LGAD arrays with noise levels below 10 pA. Their switching architectures are primarily optimized for sequential single-pixel measurements, which are well-suited for pixel-by-pixel quality control. For larger pixel arrays and a broader range of test scenarios, additional channel-routing flexibility can be beneficial. Such flexibility is particularly useful for multi-pixel measurements, row- or column-wise scans, and inter-pixel studies, where the inter-pixel configuration enables measurements of the electrical characteristics between selected pixels. A modular hardware structure can also simplify scaling, maintenance, and reconfiguration of the system. Motivated by these requirements, we developed a modular probe card system incorporating a switching architecture that enables automated characterization of large pixelated LGAD sensors with arbitrary pixel selection.

The remainder of the paper is organized as follows. Section 2 introduces the LGAD sensor from the perspective of electrical characterization and provides an overview of the evaluation system and its measurement requirements. The individual subsystems are then described in detail: the probe card in Section 3, the mechanical structure and alignment system in Section 4, the switching board in Section 5, and the control software in Section 6. The overall system performance is presented in Section 7, followed by the conclusions in Section 8.

2 System design for LGAD sensor evaluation

To meet the demands of large-scale LGAD sensor quality control, we developed a modular probe card system for reliable and efficient electrical characterization of pixelated LGAD sensors with large pixel arrays, enabling pixel-by-pixel and multi-pixel I–V and C–V measurements. This section first describes the LGAD sensor structure from the perspective of electrical characterization. The measurement objectives and system requirements are then introduced, followed by an overview of the evaluation system architecture.

Figure 1 shows a schematic diagram of a typical LGAD structure. The device is based on a modified p–i–n diode geometry that incorporates a p^+ gain layer beneath the n^{++} readout electrode. Under reverse bias, the gain layer creates a localized region of high electric field. Electrons drifting into this region undergo controlled impact ionization, producing moderate internal charge multiplication with a typical gain of 10–30. This internal gain compensates for the reduced signal charge in thin sensors and enables precise timing measurements.

The sensitive volume of the sensor is formed by a high-resistivity epitaxial layer with a thickness of approximately 50 μm . A heavily doped p^{++} substrate on the backside serves as the ohmic contact for reverse bias. On the top surface, each pixel incorporates a p^+ gain layer and an n^{++} readout electrode, with a metal contact pad formed above it. Junction Termination Extension

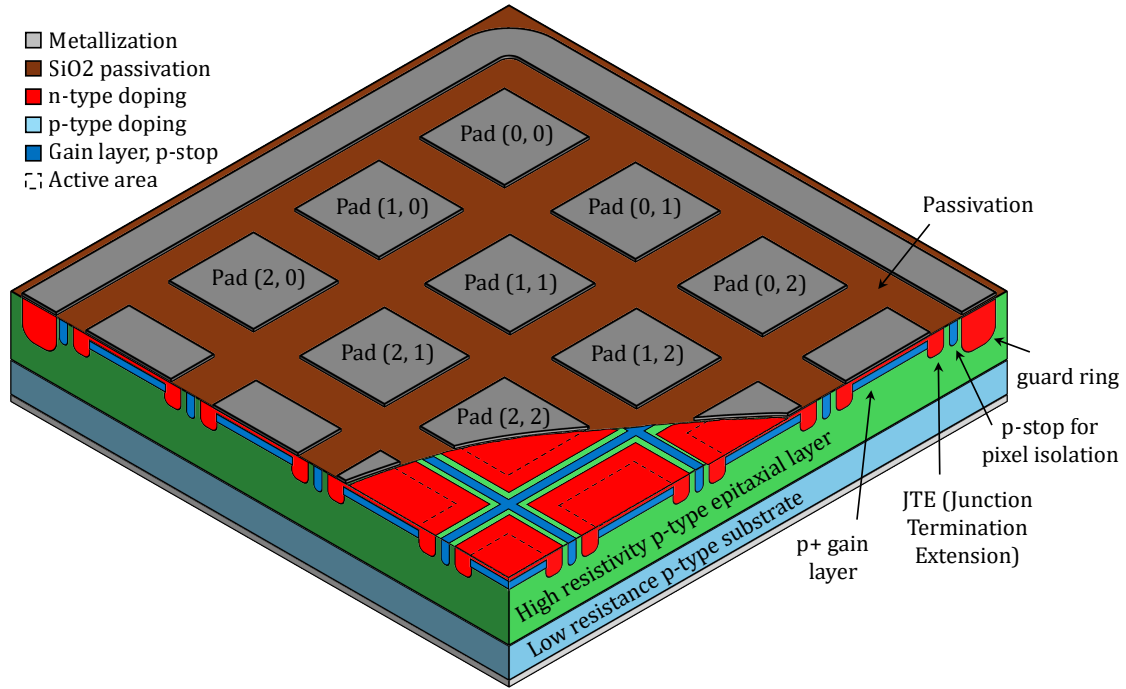


Figure 1: Schematic diagram of a typical LGAD sensor structure, showing a partial 4×4 array with a cross-sectional view. The cross-section reveals the internal layer structure from bottom to top: the low-resistivity p-type substrate serving as the ohmic contact, the high-resistivity p-type epitaxial layer forming the sensitive volume, and the p^+ gain layer and n^{++} readout electrode beneath each metal contact pad. JTE structures are implemented at the periphery of each pixel to prevent premature breakdown, and adjacent pixels and the guard ring are electrically isolated by p-stop structures. Guard rings are implemented at the sensor periphery to provide additional edge termination.

(JTE) structures are implemented at the periphery of each pixel to prevent premature breakdown. Adjacent pixels and the guard ring are electrically isolated by p-stop structures. At the sensor periphery, guard rings provide additional edge termination.

In this work, we consider LGAD sensors developed for the CMS Endcap Timing Layer, which consist of a 16×16 pixel array [15]. The key electrical characteristics of each pixel are governed by the device structure and must be measured individually to verify fabrication uniformity and ensure stable operation across the full array.

The primary objective of LGAD sensor characterization is to determine the safe operating voltage range of each pixel while ensuring sufficient internal gain for precise timing measurements. This is achieved through I–V measurements, which provide information on breakdown voltage and leakage current. In addition, C–V measurements are used to study the depletion behavior of the sensor and to assess the uniformity of the bulk and gain layer properties. These measurements define the operating conditions of the sensor and directly influence the achievable internal gain and charge collection efficiency, both of which determine the timing performance of LGAD sensors.

Based on these measurement objectives, several system requirements are identified for large-scale LGAD sensor evaluation:

- Precise and reliable pixel-level electrical characterization with low noise contribution from the readout chain
- Flexible pixel selection capability supporting single-pixel, multi-pixel, and inter-pixel measurement configurations
- Rapid measurement throughput suitable for large-scale quality control during mass production
- Cost-effective and scalable architecture for deployment across multiple institutes and testing environments

Accurate characterization requires pixel-by-pixel measurements in which the electrical response of each pixel is measured individually. During each measurement, the pixel under test must be connected to the measurement instrument while all other pixels are held at a well-defined potential, typically ground. This configuration suppresses parasitic contributions from neighboring pixels, such as electrical cross-talk and leakage current sharing, ensuring that the measured signal originates only from the selected pixel.

For sensors with a small number of pixels, such measurements can be performed using conventional probe stations equipped with needle probes. However, for sensors containing hundreds of pixels, such as the 16×16 array considered in this work, manual probing becomes impractical and difficult to scale. A dedicated probing and switching system is therefore required.

The probe card establishes electrical contact to all pixels through a pogo-pin array matched to the sensor geometry. A switching board then selectively routes the signal from a chosen pixel to the measurement instruments while grounding all other pixels. This approach enables pixel-by-pixel measurements without changing the physical probing contact and allows systematic characterization using a limited number of instrument channels.

To implement this concept, we developed an LGAD sensor evaluation system consisting of four main components: a probe card, a switching board, measurement instruments, and control software. The measurement instruments include a source-measure unit (SMU) and a picoammeter for I–V measurements, as well as an inductance–capacitance–resistance (LCR) meter for C–V measurements. The control software coordinates the switching configuration and the operation of the instruments, enabling automated scan sequences and systematic data acquisition.

Together, these components form a modular system that enables automated pixel-by-pixel electrical characterization of large pixelated LGAD sensors. An overview of the system architecture and the interaction between its components is illustrated in Fig. 2. The following sections describe each subsystem in detail.

3 Probe card

A probe card was developed to establish simultaneous electrical contact to all pixels of a 16×16 LGAD array for automated electrical characterizations. The pogo-pin layout was designed to match the geometry of LGAD sensors developed for minimum-ionizing particle (MIP) timing detectors

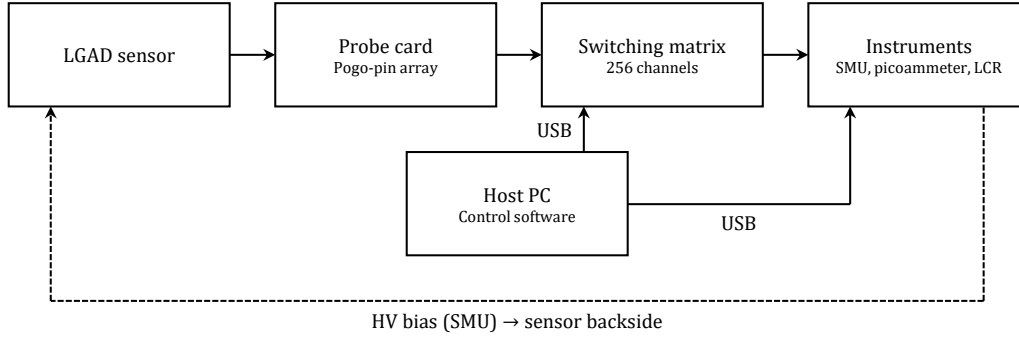


Figure 2: Block diagram of the probe card system architecture, consisting of the LGAD sensor, probe card, switching matrix, and measurement instruments. The host PC coordinates all components via USB interfaces. The SMU applies reverse bias to the sensor backside (dashed line) while pixel currents are routed through the switching matrix.

of the CMS Endcap Timing Layer (ETL). The spacing between adjacent pogo pins is 1.3 mm, corresponding to the pixel pitch of the target sensor. In addition to the 16×16 signal pins, 15 extra pogo pins were placed along one side of the array to contact the guard ring pads.

Pogo pins were selected as the contacting elements because they provide mechanically robust and repeatable contact over many measurement cycles. Compared with cantilever-type probes, pogo pins are less susceptible to permanent deformation and offer more stable contact conditions during repeated I–V and C–V scans, thereby reducing the risk of contact failure or sensor damage. The pogo pins have a spring stroke of 0.5 mm, and the full span of the pin array is 19.5 mm. These parameters determine the allowable tilt tolerance between the probe card and the sensor surface, as discussed in Section 4.

Electrical connections from the probe card to the switching board are provided through three 96-pin flexible flat cable (FFC) connectors, which carry the 256 pixel signal lines; unused connector pins are left unconnected. An FFC adapter board reorganizes these lines into sixteen 16-channel groups for connection to the motherboard of the switching system. The 15 guard ring lines are routed separately through a 20-pin FFC connector and are directly connected to ground. This separation simplifies the routing of the signal channels while keeping the guard ring at a fixed reference potential during measurements. Through this connector scheme, each pixel signal can be selectively routed by the switching board either to a measurement bus or to ground, thereby enabling flexible I–V and C–V configurations without changing the physical probing contact.

The probe card shown in Fig. 3 was designed and fabricated in collaboration with EQENG, a probe card manufacturer based in Korea. The fabricated probe card was successfully used for automated I–V and C–V measurements of 16×16 LGAD sensors, as presented in Section 7.

4 Mechanics and alignment

To establish simultaneous and reliable contact across the full 16×16 pogo-pin array, precise control of the lateral position, tilt, and vertical compression between the probe card and the sensor

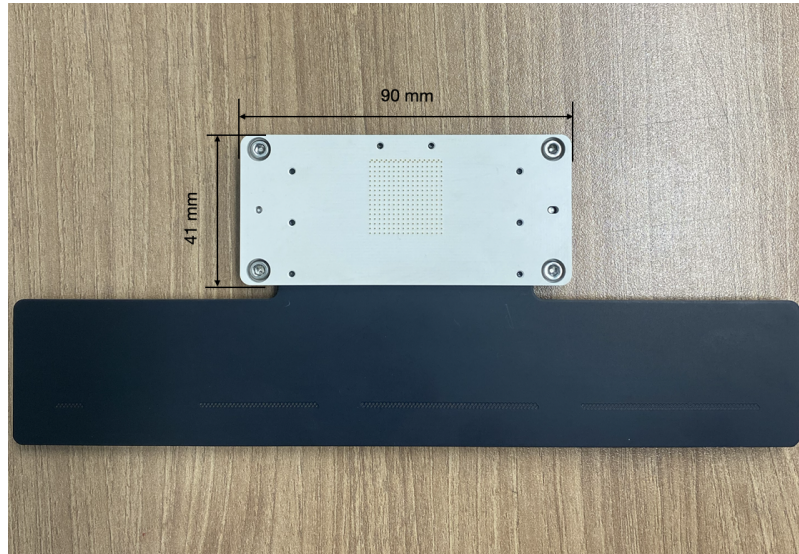


Figure 3: Fabricated probe card. The polymer head (90 mm × 41 mm) houses the central 16 × 16 pogo-pin array for pixel contact and 15 additional pogo pins for the guard ring pads. The elongated printed circuit board (PCB) section supports the FFC connectors used to route the pixel signals from the probe card to the switching board on the reverse side.

is required. A dedicated mechanical system was therefore developed for the sensor alignment and probing. The supporting structure is built from a modular aluminum profile frame, while fine positioning and angular adjustments are provided by precision motion stages. The sensor is mounted on a vacuum chuck to ensure stable positioning during the probing procedure.

The jig system, shown in Fig. 4, consists of an upper assembly that supports the probe card and a lower assembly that carries the sensor on the vacuum chuck together with the positioning stages. This separation allows the probe card to remain mechanically stable while the sensor position is adjusted with respect to it. Dedicated holders are mounted on the frame for auxiliary components, including the alignment cameras and the FFC adapters. These components are fixed directly to the aluminum profiles to maintain their relative position with respect to the probe card and sensor during alignment and measurement.

For alignment, two reference holes in the probe card are matched to corresponding patterns on the sensor. Two top-view cameras are used to monitor these alignment marks and to adjust the lateral position and in-plane rotation between the probe card and the sensor. To monitor the relative tilt, two additional side-view cameras are placed along the x and y directions of the sensor plane. Alignment is performed by first correcting the x–y position and rotation using the top-view images, then adjusting the tilt using the side-view images, and finally approaching the sensor in the z direction to achieve controlled compression of the pogo pins.

The stage specifications were selected based on the alignment tolerances imposed by the sensor pad geometry and the pogo-pin contact conditions. XY, Z, tilt, and rotation stages with a positioning resolution of 10 μm are employed. This resolution is well below the characteristic dimensions of the sensor contact pads, which have typical dimensions of approximately 200 μm × 100 μm. This

resolution also satisfies the vertical direction requirement that is set by the pogo-pin spring stroke of about 500 μm , which determines the allowable range for controlled compression during probing.

Based on the pogo-pin stroke of 0.5 mm and the full pin-array span of 19.5 mm (Section 3), the height variation across the array must remain within the available spring stroke to ensure that all pins can make contact without over-compression. This condition corresponds to an allowable tilt of approximately 1.4° between the probe card and the sensor surface. To satisfy this requirement, a tilt stage with an angular resolution of 0.3° is used in the probing setup.

A similar geometric consideration applies to the in-plane rotation. From the pad dimensions and the full lateral extent of the sensor, an allowable rotational tolerance of approximately 0.5° is sufficient to keep the contact displacement within the pad area.

The complete probing setup is operated inside a light-tight enclosure during measurements, due to visible-wavelength photons being absorbed in the silicon sensor that generate electron-hole pairs, producing photocurrent that can distort both I-V and C-V measurements. The enclosure therefore suppresses photo-induced current and ensures that the measured response reflects the intrinsic electrical properties of the sensor.

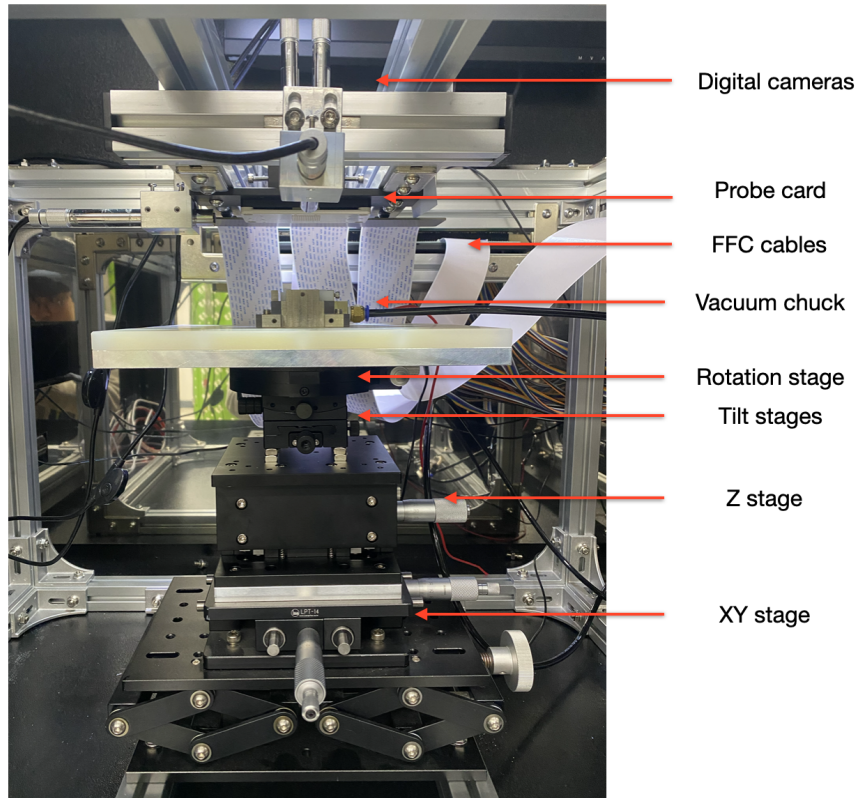


Figure 4: Probing setup used for precise alignment between the probe card and the sensor. The upper assembly supports the probe card and alignment cameras, while the lower assembly carries the sensor on a vacuum chuck together with the multi-axis positioning stages. FFC cables connect the probe card to the switching board.

5 Switching board

To enable automated I–V and C–V measurements of LGAD sensors with a 16×16 pixel array, a dedicated switching board was developed. Its primary function is to connect selected pixels to the external measurement instruments while holding all non-selected pixels at ground potential. This configuration suppresses unwanted contributions from neighboring pixels and enables systematic pixel-by-pixel characterization without changing the physical probing contact or manually reconnecting cables. In addition, the switching architecture supports flexible measurement configurations beyond single-pixel access, as described below.

The switching system is implemented as a modular matrix providing 256 independent channels. It consists of 16 unit boards, each handling 16 channels, mounted on a single motherboard. Each channel corresponds to one LGAD pixel, allowing the full 16×16 sensor array to be addressed through a common hardware platform. This modular organization simplifies assembly, maintenance, and possible future adaptation to other sensor layouts.

The overall switching concept was inspired by previously reported multi-channel LGAD switching schemes [13], in which switches and multiplexers are combined to access individual pixels. In the present design, a simplified architecture based solely on analog switches was adopted and combined with four independent measurement buses. This approach increases routing flexibility for multi-pixel and inter-pixel measurements, at the cost of introducing a small additional offset or leakage contribution from the shared signal paths. As discussed in Section 7, this contribution was found to be small compared with the leakage current typically observed for functional LGAD pixels.

Analog switches (TMUX1134¹, Texas Instruments) were selected as the core switching elements. Each device integrates four bidirectional single-pole double-throw (SPDT) switches in a single package and provides low on-resistance with a typical channel leakage current of about 50 pA. The SPDT configuration is particularly useful because it allows each pixel either to be routed to a measurement bus or to be tied to ground. This ensures that only the selected pixel contributes to the measured signal, while all other pixels remain at a well-defined reference potential during the measurement.

A unit board serves as the basic building block of the switching matrix. Each unit board contains four TMUX1134 chips, corresponding to 16 independent switching channels. For each channel, the probe-card signal line is connected to the common terminal of the switch, while the two switched outputs are connected to a measurement bus and to ground, respectively. This unit-level modularity simplifies the printed circuit board (PCB) layout, keeps the sensitive analog paths short, and allows individual boards to be replaced or reconfigured when needed. The schematic diagram and a photograph of the fabricated unit board are shown in Fig. 5.

The motherboard, shown in Fig. 6, hosts 16 unit boards and provides a total of 256 switching channels. It distributes the signal lines from the probe card together with the common ground, digital control signals, and power required by the unit boards. The 256 pixel signals are transferred from the probe card through three 96-pin FFC connectors to an FFC adapter board, which reorganizes them into sixteen 16-channel groups. These groups are then connected to the motherboard through

¹<https://www.ti.com/product/ko-kr/TMUX1134>

eight 32-pin connectors, each serving two 16-channel groups. The motherboard routes the selected signals to four independent measurement buses connected to the external instruments.

This four-bus architecture supports several measurement modes, including single-pixel, multi-pixel, row-wise, and column-wise configurations. Because each channel can be switched independently and adjacent pixels are assigned to different buses, arbitrary pixel selection and simultaneous multi-pixel access are both possible while the remaining pixels are held at ground. This flexibility is useful for routine pixel-by-pixel quality control, rapid pre-scans, and inter-pixel measurements, in which neighboring pixels can be connected to different buses so that the instrument probes the electrical path between them.

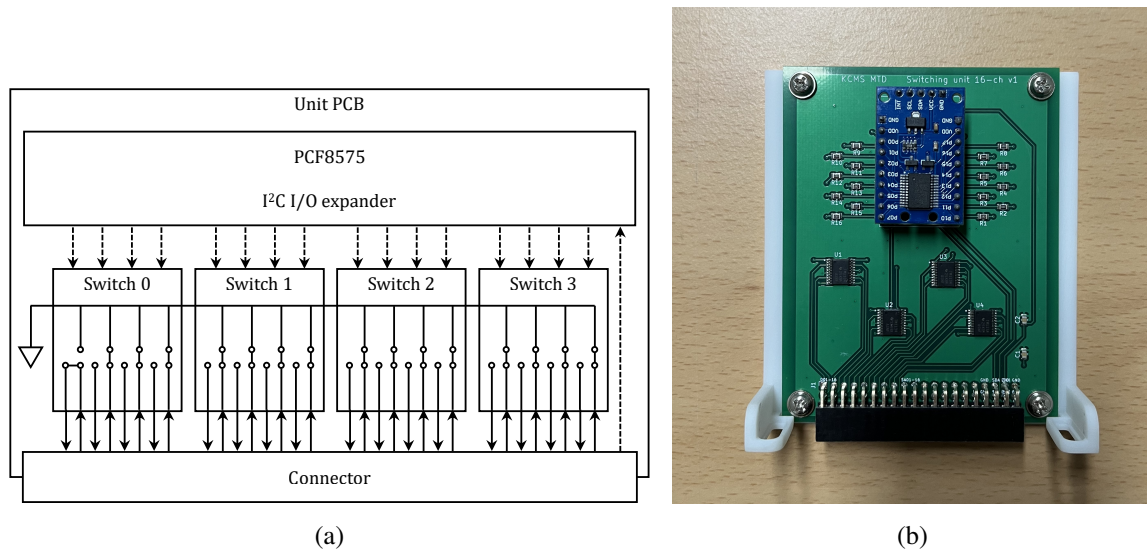


Figure 5: Unit board (a) Schematic diagram. One unit board integrates four 4-channel analog switches together with a PCF8575 I/O expander for digital control via I²C. (b) Fabricated unit board.

To control the large number of switching channels, each unit board integrates a PCF8575² I/O expander together with the analog switches. Each PCF8575 provides 16 digital output lines for controlling the corresponding 16 switching channels via the I²C protocol. A Raspberry Pi Pico based on the RP2040³ microcontroller serves as the main controller, communicating with the PCF8575 devices via I²C and with the host PC through a USB interface. Because the RP2040 provides two independent I²C controllers and the PCF8575 supports up to eight selectable addresses per bus, all 16 unit boards can be controlled with a single microcontroller.

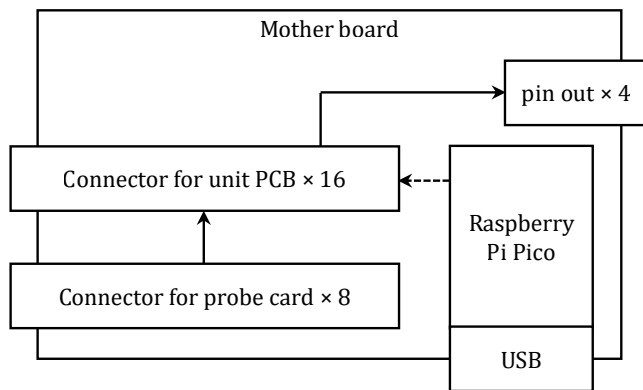
Control software running on the host PC coordinates the switching configuration and synchronizes it with the external measurement instruments. For I–V measurements, a SMU⁴ and a picoammeter⁵ are used. The SMU applies reverse bias to the backside of the sensor and monitors

²<https://www.ti.com/product/PCF8575>

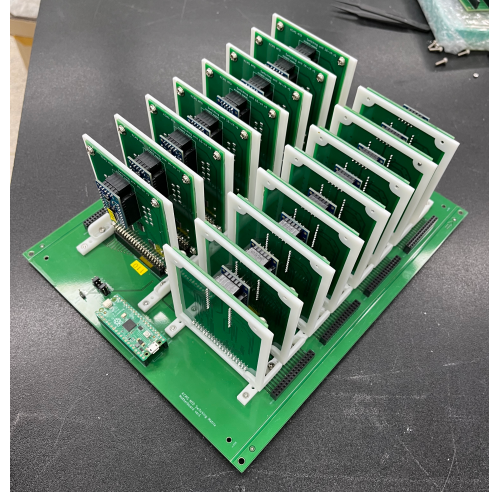
³<https://www.raspberrypi.com/products/rp2040/>

⁴<https://www.tek.com/ko/products/keithley/source-measure-units/2400-standard-series-sourcemeater>

⁵<https://www.tek.com/ko/products/keithley/low-level-sensitive-and-specialty-instruments/series-6400-picoammeters>



(a)



(b)

Figure 6: Motherboard of the switching system. (a) Schematic diagram of the motherboard, illustrating the connections between the probe card, the unit PCBs, the four output pins to the external measurement instruments, and the Raspberry Pi Pico microcontroller used for switch control and USB communication with the host PC. (b) Assembled switching system, showing the modular implementation with the unit PCBs mounted vertically on the motherboard.

the total current of the full array, while the picoammeter measures the current from the selected pixel or pixel group routed through the switching matrix. Typical I–V scans extend up to approximately 300 V, depending on the sensor under test.

To protect the sensor during the bias sweep, the current compliance of the SMU is used as a hardware safety limit. When the measured current reaches the compliance threshold, the control software immediately initiates a return sweep to 0 V. This prevents excessive current flow near breakdown and shortens the measurement time for channels that show an early current rise.

For C–V measurements, a Wayne Kerr 43100⁶ LCR meter is used, providing capacitance resolution down to 10^{-5} pF and an internal DC bias of up to 40 V. For measurements requiring a higher bias voltage, an external DC source can be added in series between the switching matrix and the LCR meter.

6 Software Design

The characterization of large pixelated LGAD sensors, such as the 16×16 array considered in this work, requires coordinated control of the switching matrix and the precision measurement instruments, together with automated scan execution and stable remote operation. To meet these requirements, dedicated control software was developed with the following technical objectives:

- Ensure synchronized control of the switching matrix and the measurement instruments, so that the electrical path configuration remains consistent with the measurement sequence.

⁶https://www.waynekerrtest.com/products_detail.php?indexs=7&brand=Wayne%20Kerr

- Support fully automated scan sequences over all 256 channels to minimize manual intervention and improve measurement consistency.
- Provide both a graphical user interface (GUI) for interactive monitoring and a command-line interface (CLI) for terminal-based operation and scripted automation.
- Enable stable remote access to the measurement system, allowing operation without direct physical proximity to the hardware setup.

To satisfy these requirements, the software was implemented using a server-client architecture. This decoupled design improves modularity and allows the user interface to run on a different network node from the measurement server. Communication between the server and the clients is implemented through the WebSocket protocol using JSON-formatted messages. The overall architecture of the software system, including the interaction between the server and multiple clients, is illustrated in Fig. 7.

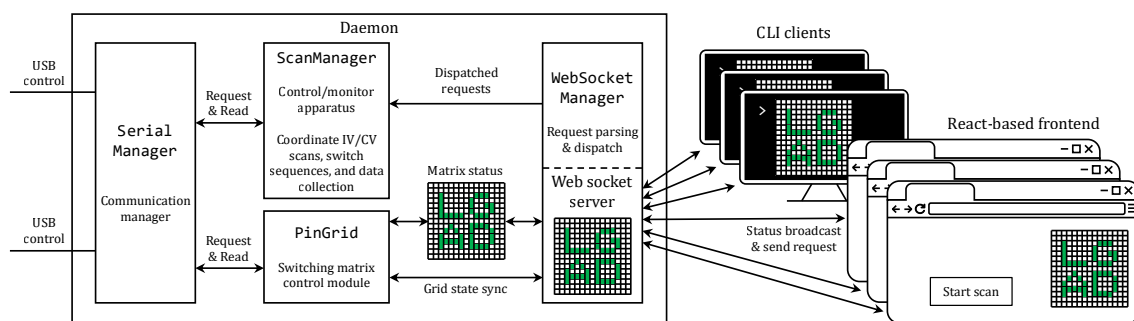


Figure 7: Block diagram of the software architecture. The server runs as a Linux daemon and consists of four main components: `SerialManager`, which communicates with the switching hardware and measurement instruments; `ScanManager`, which coordinates automated I–V and C–V scans; `PinGrid`, which maintains the switching-matrix state; and `WebSocketManager`, which handles communication with connected clients. Both GUI and CLI clients can monitor the system state and interact with the server in real time.

The server is implemented in C++ and runs as a background Linux daemon to provide continuous access to the measurement system. At startup, it automatically establishes communication with the Raspberry Pi Pico and the connected measurement instruments. Its core functionality is organized into four main software components:

- `PinGrid`: maintains the logical state of the 16×16 switching matrix and keeps the software-defined channel configuration consistent with the physical switch states.
- `SerialManager`: handles low-level serial communication with the switching hardware and the external measurement instruments.
- `WebSocketManager`: manages client connections, parses incoming requests, and distributes updated system status information.

- **ScanManager**: coordinates automated I–V and C–V scan sequences, including predefined scan modes ranging from full-array scans to selected regions of interest.

The server supports simultaneous connections from multiple clients. When more than one client is connected, the current system state, including the switching-matrix configuration, is synchronized across all active interfaces in real time.

Two complementary client interfaces were developed for interaction with the server. The GUI client is a web-based application built with the React library⁷, providing a visual representation of the 16×16 pixel grid. It allows users to monitor the real-time channel status, inspect the switching configuration, initiate scan sequences, and view system logs. The CLI client supports operation in environments without a graphical desktop and is particularly useful for scripting and integration into broader automated testing workflows.

7 Performance

The developed system was validated through automated I–V and C–V measurements of a 16×16 LGAD array. In a typical measurement sequence, the probe card is first aligned to the sensor and electrical contact is established. A target pixel or pixel group is then selected through the switching matrix, after which an I–V or C–V curve is acquired by a voltage sweep. The measured data are stored in plain text format, and the system then proceeds to the next channel configuration by returning to the channel-selection step. This sequence is repeated until all designated channels are scanned.

As a rapid pre-screening step, row-wise I–V measurements were first performed by connecting all pixels within a row simultaneously. With this configuration, the full 16×16 array could be scanned in approximately 20 minutes, providing a quick overview of the row-level I–V of the sensor. Figure 8(a) shows the resulting I–V curves for each row, and Fig. 8(b) shows the corresponding row-status map. Rows composed entirely of functional pixels are shown in green, rows containing pixels with moderately early breakdown are shown in orange, and rows containing one or more pixels with significant premature breakdown are shown in red.

Following the row-wise pre-screening, pixel-by-pixel I–V measurements were performed for detailed characterization of the full array. For a voltage sweep from 0 to 300 V with a 1 V step, the full 16×16 scan required approximately 340 minutes. Figure 9(a) shows the I–V curves measured for all pixels, and Fig. 9(b) shows the corresponding pixel-status map. Each pixel is classified into three categories based on its breakdown behavior relative to the designed operating voltage of approximately 250 V: functional pixels are shown in green, pixels with moderately early breakdown are shown in orange, and pixels with significantly premature breakdown are shown in red.

This two-stage approach demonstrates a practical measurement strategy for large-scale LGAD quality control. The rapid row-wise scan, completed in approximately 20 minutes, provides an efficient pre-screening step for identifying rows that require closer inspection. A subsequent pixel-by-pixel scan can then be focused on the flagged rows, rather than being applied to the entire array from the outset. For the measurement conditions used here, this significantly improves the efficiency of sensor characterization compared with performing a full-array pixel-by-pixel scan alone.

⁷<https://react.dev>

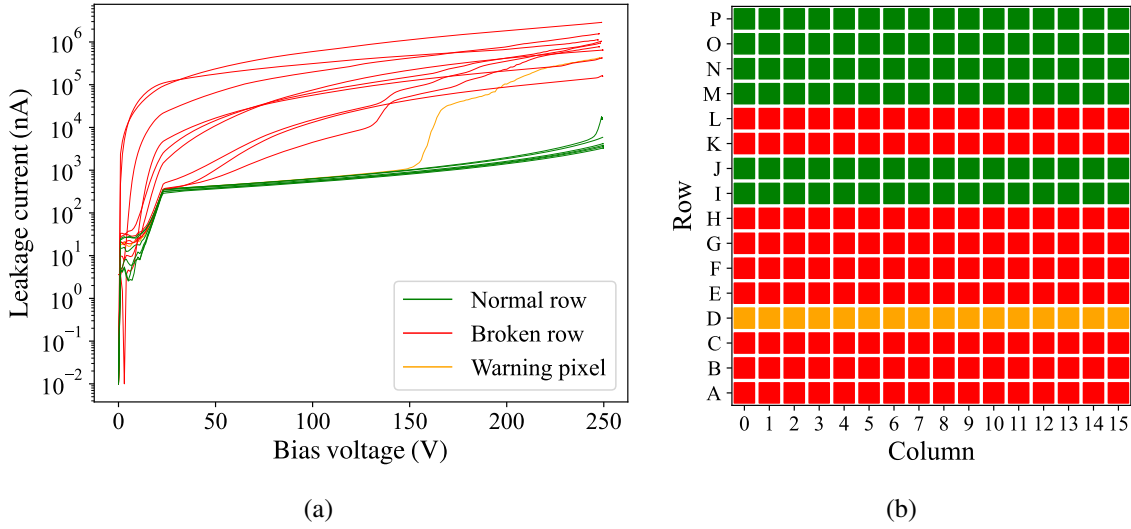


Figure 8: I-V measurement results from the row-wise scan of a 16×16 LGAD array. (a) I-V curves measured for each row, with rows classified as normal (green), warning (orange), or broken (red) based on the breakdown behavior of the pixels within the row. (b) Row-status map of the full array. Rows are classified as broken if they contain one or more pixels with significant premature breakdown, and as warning if they contain pixels with moderately early breakdown.

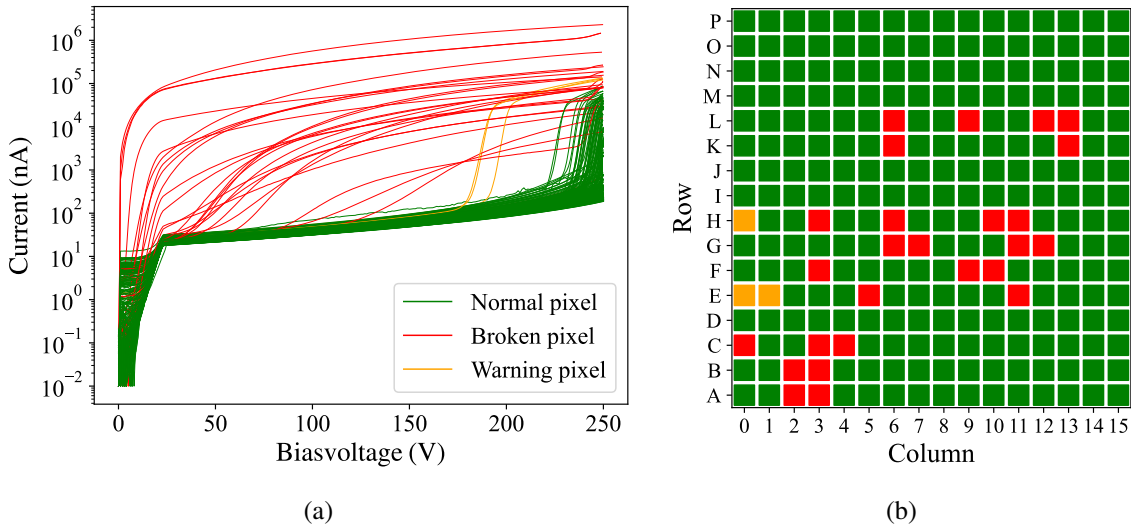


Figure 9: I-V measurement results from the pixel-by-pixel scan of a 16×16 LGAD array. (a) I-V curves measured for all pixels, with pixels classified as normal (green), warning (orange), or broken (red) according to their breakdown behavior relative to the designed operating voltage of approximately 250 V. (b) Pixel-status map of the full array showing the spatial distribution of each pixel category.

To evaluate the offset and noise introduced by the switching matrix, the leakage current of a single LGAD pixel was measured both with and without the switching matrix in the readout path. In the reference configuration, the picoammeter was connected directly to the pixel. In the switch configuration, the same signal was routed through the switching matrix. Figure 10 shows the measured current as a function of time for both cases. Without the switching matrix, the measured current has a standard deviation of 0.066 nA. With the switching matrix, an offset of approximately 0.46 nA is introduced and the standard deviation increases to 0.19 nA. Even in the extreme case where all 256 outputs are connected to a single readout channel, the total leakage current contribution from the switching matrix remains below 1 nA. These values remain small compared with the typical leakage current of a normal LGAD pixel, indicating that the switching matrix does not significantly degrade the measurement quality.

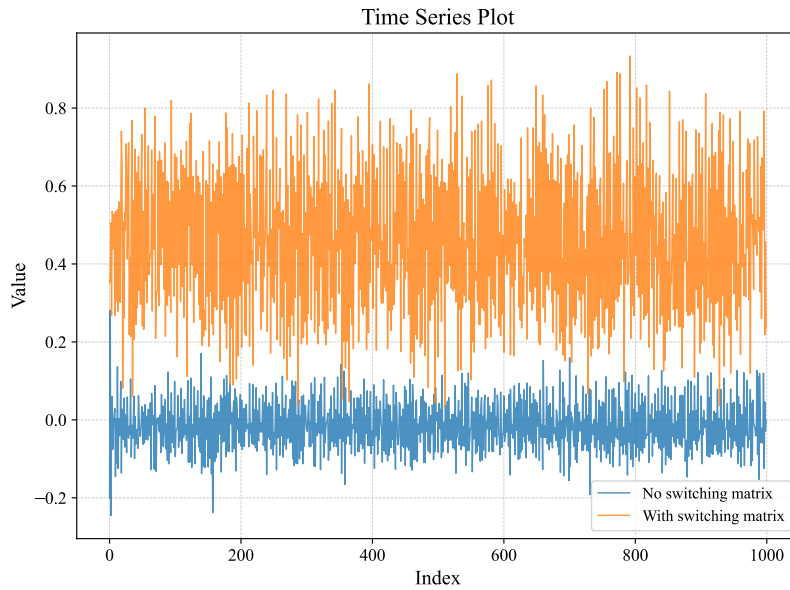


Figure 10: Comparison of the measured leakage current with and without the switching matrix in the readout path. The picoammeter was connected directly to a single LGAD pixel in the reference configuration (blue), and the same signal was routed through the switching matrix in the switched configuration (orange). The switching matrix introduces an offset of approximately 0.46 nA and increases the standard deviation from 0.066 nA to 0.19 nA.

Pixel-by-pixel C–V measurements were also performed for the same sensor. For a bias sweep up to 40 V, each channel required approximately one minute, with the scan speed primarily limited by the performance of the LCR meter. Figure 11(a) shows the C–V curves measured for all pixels, and Fig. 11(b) shows the corresponding pixel-status map. Normal pixels exhibit consistent C–V characteristics with a clear depletion transition, whereas broken pixels do not show a well-defined C–V curve and instead exhibit large capacitance fluctuations over the full bias range.

The pixel-status maps obtained from the I–V and C–V measurements do not necessarily coincide, because the two measurements probe different electrical characteristics of the sensor. In particular, the C–V scan in this study was limited to 40 V, whereas the I–V scan was used to evaluate breakdown behavior near the operating voltage. As a result, pixels showing premature breakdown

in the I–V measurement can still exhibit a well-defined C–V response within the lower voltage range covered by the C–V scan.

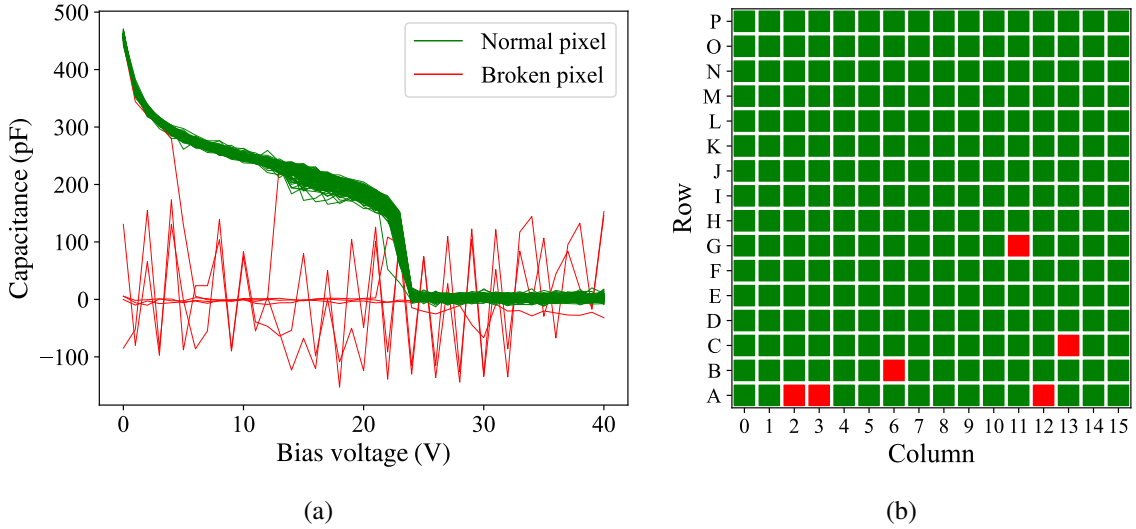


Figure 11: C–V measurement results from the pixel-by-pixel scan of a 16×16 LGAD array. (a) C–V curves measured for all pixels, with pixels classified as normal (green) or broken (red) according to the presence or absence of a well-defined depletion transition. (b) Pixel-status map of the full array showing the spatial distribution of the two categories.

8 Conclusions

We have developed and validated an automated probe card system for the electrical characterization of full-size pixelated LGAD sensors. The system is designed for 16×16 LGAD arrays and supports automated row-wise and pixel-by-pixel I–V and C–V measurements, addressing the need for reliable and scalable quality control in high-granularity timing-detector applications.

The developed platform combines a pogo-pin probe card matched to the sensor geometry, a 256-channel modular switching matrix, precision measurement instruments, and integrated control software based on a server-client architecture. The switching system enables selective access to individual pixels while holding non-selected pixels at ground, and also supports multi-pixel row-wise measurement configurations. The additional offset and leakage introduced by the switching matrix remain small compared with the leakage current of a normal LGAD pixel, showing that the switching architecture does not significantly degrade the measurement quality.

Automated measurements of a 16×16 LGAD array were successfully demonstrated with the system. A row-wise I–V scan of the full array was completed in approximately 20 minutes, while a pixel-by-pixel I–V scan from 0 to 300 V with a 1 V step required about 340 minutes. This enables a practical two-stage workflow in which rapid pre-screening is followed by a detailed inspection of flagged regions, thereby improving the efficiency of large-scale sensor characterization.

These results demonstrate that the developed system provides a practical and scalable solution for LGAD quality control. Its modular hardware design, flexible switching architecture, and

automation capability make it well-suited for use in distributed sensor testing environments and future large-scale LGAD production and evaluation campaigns.

Acknowledgments

This work is supported by the National Research Foundation of Korea (NRF) grants funded by the Korea government (MSIT) (RS-2008-NR007227, RS-2020-NR050645, and RS-2025-00560964) and a Korea University Grant.

References

- [1] G. Pellegrini, P. Fernández-Martínez, M. Baselga, C. Fleta, D. Flores, V. Greco, S. Hidalgo, I. Mandić, G. Kramberger, D. Quirion, and M. Ullan. Technology developments and first measurements of low gain avalanche detectors (lgad) for high energy physics applications. *Nuclear Instruments and Methods in Physics Research Section A: Accelerators, Spectrometers, Detectors and Associated Equipment*, 765:12–16, 2014. ISSN 0168-9002. doi: <https://doi.org/10.1016/j.nima.2014.06.008>. URL <https://www.sciencedirect.com/science/article/pii/S0168900214007128>. HSTD-9 2013 - Proceedings of the 9th International "Hiroshima" Symposium on Development and Application of Semiconductor Tracking Detectors.
- [2] Fabio Ravera. The CT-PPS project: detector hardware and operational experience. *PoS, Vertex 2017*: 015, 2018. doi: 10.22323/1.309.0015.
- [3] N. Cartiglia, A. Staiano, V. Sola, R. Arcidiacono, R. Cirio, F. Cenna, M. Ferrero, V. Monaco, R. Mulargia, M. Obertino, F. Ravera, R. Sacchi, A. Bellora, S. Durando, M. Mandurrino, N. Minafra, V. Fadeyev, P. Freeman, Z. Galloway, E. Gkougkousis, H. Grabas, B. Gruey, C.A. Labitan, R. Losakul, Z. Luce, F. McKinney-Martinez, H.F.-W. Sadrozinski, A. Seiden, E. Spencer, M. Wilder, N. Woods, A. Zatserklyaniy, G. Pellegrini, S. Hidalgo, M. Carulla, D. Flores, A. Merlos, D. Quirion, V. Cindro, G. Kramberger, I. Mandić, M. Mikuž, and M. Zavrtanik. Beam test results of a 16ps timing system based on ultra-fast silicon detectors. *Nuclear Instruments and Methods in Physics Research Section A: Accelerators, Spectrometers, Detectors and Associated Equipment*, 850:83–88, 2017. ISSN 0168-9002. doi: <https://doi.org/10.1016/j.nima.2017.01.021>. URL <https://www.sciencedirect.com/science/article/pii/S0168900217300219>.
- [4] M. Berretti, R. Arcidiacono, E. Bossini, M. Bozzo, N. Cartiglia, M. Ferrero, V. Georgiev, T. Isidori, R. Linhart, N. Minafra, M.M. Obertino, V. Sola, and N. Turini. Test of ultra fast silicon detectors for the totem upgrade project. *Journal of Instrumentation*, 12(03):P03024, mar 2017. doi: 10.1088/1748-0221/12/03/P03024. URL <https://doi.org/10.1088/1748-0221/12/03/P03024>.
- [5] Joaquim Pinol. The high-granularity timing detector for atlas at hl-lhc. *Particles*, 8(2), 2025. ISSN 2571-712X. doi: 10.3390/particles8020036. URL <https://www.mdpi.com/2571-712X/8/2/36>.
- [6] *Precision Timing with the CMS MTD Endcap Timing Layer for HL-LHC*. doi: 10.7566/JPSCP.34.010013. URL <https://journals.jps.jp/doi/abs/10.7566/JPSCP.34.010013>.
- [7] M. Ferrero. The cms mtd endcap timing layer: Precision timing with low gain avalanche diodes. *Nuclear Instruments and Methods in Physics Research Section A: Accelerators, Spectrometers, Detectors and Associated Equipment*, 1032:166627, 2022. ISSN 0168-9002. doi:

<https://doi.org/10.1016/j.nima.2022.166627>. URL

<https://www.sciencedirect.com/science/article/pii/S0168900222001991>.

- [8] J. Pietraszko, T. Galatyuk, V. Kedych, M. Kis, W. Koenig, M. Koziel, W. Krüger, R. Lalik, S. Linev, J. Michel, S. Moneta, A. Rost, A. Schemm, C. J. Schmidt, K. Sumara, M. Träger, M. Traxler, and Ch. Wendisch. Low gain avalanche detectors for the hades reaction time (T_0) detector upgrade. *The European Physical Journal A*, 56(7):183, 2020.
- [9] C. Bishop, A. Das, J. Ding, M. Gignac, F. Martinez-McKinney, S.M. Mazza, A. Molnar, N. Nagel, M. Nizam, J. Ott, H.F.-W. Sadrozinski, B. Schumm, A. Seiden, T. Shin, A. Summerell, M. Wilder, and Y. Zhao. Long-distance signal propagation in ac-Igad. *Nuclear Instruments and Methods in Physics Research Section A: Accelerators, Spectrometers, Detectors and Associated Equipment*, 1064:169478, 2024. ISSN 0168-9002. doi: <https://doi.org/10.1016/j.nima.2024.169478>. URL <https://www.sciencedirect.com/science/article/pii/S0168900224004042>.
- [10] Miles Davis, Graeme Stage, Alice Borjigin, Sienna Beringer, Nolan Lynch, Simon Nakarmi, Carmen Galmes Altafulla, Alexander Drumm, Adam Molnar, Aidan Tiernan, Simone Mazza, Hartmut Sadrozinski, Bruce Schumm, Abraham Seiden, Forest MartinezMckinney, and Taylor Shin. Characterization of the first full-size production for ePIC TOF layers. *PoS, VERTEX2025:020*, 2025. doi: 10.22323/1.513.0020.
- [11] L. Cavazzini, A. Bisht, M. Boscardin, M. Centis Vignali, F. Ficorella, M. Fernandez Garcia, O. Hammad Ali, M. Moll, G. Paternoster, and M. Wiehe. Development and characterization of large area Igads for space applications. *Journal of Instrumentation*, 20(07):C07049, jul 2025. doi: 10.1088/1748-0221/20/07/C07049. URL <https://doi.org/10.1088/1748-0221/20/07/C07049>.
- [12] Ryan Heller, Justin Ellin, Michael Backfish, Joshua W. Cates, Woon-Seng Choong, Nicolaus Kratochwil, Eric Prebys, Leonor Rebolo, Sara St. James, and Gerard Ariño-Estrada. Demonstration of Igads and cherenkov gamma detectors for prompt gamma timing proton therapy range verification. *IEEE Transactions on Radiation and Plasma Medical Sciences*, 9(4):508–514, 2025. doi: 10.1109/TRPMS.2024.3494720.
- [13] J.J. Ge, X. Yang, X.X. Zheng, Z. Galloway, C. Gee, M. Wilder, W. Wyatt, C.H. Li, H. Liang, and Y.W. Liu. Digital switch boards for iv and cv measurements of large-array low gain avalanche detectors. *Nuclear Instruments and Methods in Physics Research Section A: Accelerators, Spectrometers, Detectors and Associated Equipment*, 1005:165400, 2021. ISSN 0168-9002. doi: <https://doi.org/10.1016/j.nima.2021.165400>. URL <https://www.sciencedirect.com/science/article/pii/S0168900221003843>.
- [14] X. Yang, S. Alderweireldt, N. Atanov, M.K. Ayoub, J. Barreiro Guimaraes da Costa, L. Castillo García, H. Chen, S. Christie, V. Cindro, H. Cui, G. D’Amen, Y. Davydov, Y.Y. Fan, Z. Galloway, J.J. Ge, C. Gee, G. Giacomini, E.L. Gkougkousis, C. Grieco, S. Grinstein, J. Grosse-Knetter, S. Guindon, S. Han, A. Howard, Y.P. Huang, Y. Jin, M.Q. Jing, R. Kiuchi, G. Kramberger, E. Kuwertz, C. Labitan, J. Lange, M. Leite, C.H. Li, Q.Y. Li, B. Liu, J.Y. Liu, Y.W. Liu, H. Liang, Z.J. Liang, M. Lockerby, F. Lyu, I. Mandić, F. Martinez-Mckinney, S.M. Mazza, M. Mikuž, R. Padilla, B.H. Qi, A. Quadt, K.L. Ran, H. Ren, C. Rizzi, E. Rossi, H.F.-W. Sadrozinski, G.T. Saito, B. Schumm, M. Schwickardi, A. Seiden, L.Y. Shan, L.S. Shi, X. Shi, A. Soares Canas Ferreira, Y.J. Sun, Y.H. Tan, A. Tricoli, G.Y. Wan, M. Wilder, K.W. Wu, W. Wyatt, S.Y. Xiao, T. Yang, Y.Z. Yang, C.J. Yu, L. Zhao, M. Zhao, Y. Zhao, Z.G. Zhao, X.X. Zheng, and X.A. Zhuang. Layout and performance of hpk prototype lgad sensors for the high-granularity timing detector. *Nuclear Instruments and Methods in Physics Research Section A: Accelerators, Spectrometers, Detectors and Associated Equipment*, 980:164379,

2020. ISSN 0168-9002. doi: <https://doi.org/10.1016/j.nima.2020.164379>. URL
<https://www.sciencedirect.com/science/article/pii/S0168900220307762>.

- [15] Collaboration CMS. A MIP Timing Detector for the CMS Phase-2 Upgrade. Technical report, CERN, Geneva, 2019. URL <https://cds.cern.ch/record/2667167>.